EUROPEAN ORGANIZATION FOR NUCLEAR RESEARCH

L3 Note 2747
June 24, 2002

Charged Lepton-Pair Production in Two-Photon Collisions at LEP

L3 Collaboration

Abstract

The QED process $e^+e^- \rightarrow e^+e^-l^+l^-$ is a dominant channel at LEP2. It is studied with the L3 detector for $\ell = e$, μ and τ using an untagged data sample collected at the center-of-mass energies $161 \leq \sqrt{s} \leq 208$ GeV. The τ pairs are observed through the $\tau^+ \rightarrow \pi^+\pi^0\bar{\nu_\tau}$ and $\tau^- \rightarrow e^-\nu_\tau\bar{\nu_e}$ decay channels. Preliminary results for the cross sections are given as a function of $\sqrt{s}$ and the two-photon mass for $3 \leq W_{\gamma\gamma} \leq 40$ GeV. Good agreement is found between these measurements and the QED expectations computed to $\mathcal{O}(\alpha^4)$. In addition preliminary limits on the anomalous magnetic and electric moments of the τ lepton have been extracted.

Submitted to the 31st *International Conference on High Energy Physics*
Amsterdam, Netherlands, 24-31 July 2002.

1 Introduction

Charged lepton-pair production in two-photon collisions offers an efficient tool to test QED computations to order $\mathcal{O}(\alpha^4)$ over a wide kinematical range. The reactions are $e^+e^- \to e^+e^-e^+e^-$, $e^+e^- \to e^+e^-\mu^+\mu^-$ and $e^+e^- \to e^+e^-\tau^+\tau^-$. The diagrams which contribute at the lowest order are shown in Figure 1, they correspond to 36 diagrams for e^+e^- pairs and 12 for $\mu^+\mu^-$ and $\tau^+\tau^-$ pairs.

The study of the process $\gamma\gamma \to \tau^+\tau^-$ at LEP can be used to measure the anomalous magnetic and electric moments of the τ lepton as proposed in Ref. [1]. The anomalous magnetic moment μ_τ and electric moment d_τ are defined as

$$\mu_\tau = \frac{e(1+F_2(0))}{2m_\tau} \quad \text{and} \qquad d_\tau = -\frac{eF_3(0)}{2m_\tau}. \tag{1}$$

They depend on the form-factor F_2 and F_3 at $Q^2 = 0$ which are directly measured in no-tag two-photon processes. Moreover, since $\gamma\gamma \to \tau^+\tau^-$ at lowest order is a pure QED process, there is no contamination from other couplings, such as $Z\tau\tau$. Both couplings are related in a $SU(2) \times U(1)$ symmetry. Indeed, the relations shown in Equation 1 have been used to extract stringent bounds on the anomalous moments from measurements of $Z \to \tau^+\tau^-$ at LEP [2]. Thus, independent measurements of the anomalous magnetic and electric moments and $Z\tau\tau$ couplings provide a test of these class of models.

For an e^+e^- center-of-mass energy $\sqrt{s}$ close to the Z mass, the L3 collaboration has studied the $e^+e^- \to e^+e^-l^+l^-$ reactions where $l = e, \mu$ or τ for untagged two-photons events. The integrated luminosities were 52 pb^{-1} for the e^+e^- and $\mu^+\mu^-$ channels and of 112 pb^{-1} for the $\tau^+\tau^-$ channel [4]. Good agreement was found between the measurement and the QED expectations at $\mathcal{O}(\alpha^4)$.

The lepton production is studied as a function of the two-photon mass $\text{W}_{\gamma\gamma}$ in the range 161 GeV $\leq \sqrt{s} \leq$ 208 GeV. The individual energies and luminosities are listed in Table 1. The integrated luminosity for the analysis of the μ pairs is lower than in the case of the τ pairs, because of problems in the muon chambers during the last 3 years of data taking. The two-photon production of τ-pairs was also measured by OPAL in single tagged mode [5].

In this note, only the $\mu^+\mu^-$ and $\tau^+\tau^-$ channels are presented.

2 The L3 Detector

The L3 detector [6] consists of the following elements: a silicon microvertex detector, a central tracking chamber (TEC), a high resolution electromagnetic calorimeter (ECAL) composed of BGO crystals, a lead-scintillator ring calorimeter at low polar angles, a scintillation counter system, a uranium hadron calorimeter with proportional chamber readout (HCAL) and an accurate muon spectrometer. Forward-backward muon chambers extend the polar angle coverage of the muon system down to 24 degrees with respect to the beam line. All detectors are installed in a 12 m diameter magnet which provides a solenoidal field of 0.5 T in the central region and a toroidal field of 1.2 T in the forward-backward region. The luminosity is measured using two small BGO calorimeters preceded by silicon trackers situated on each side of the detector.

3 Monte Carlo Simulation

$e^+e^- \to e^+e^-\mu^+\mu^-$

In order to calculate the signal efficiencies and background contribution and to compare the data to the prediction of QED, the DIAG36 [7] generator is used at each center-of-mass energy. The DIAG36 program calculates the full set of diagrams to $\mathcal{O}(\alpha^4)$, taking into account the bremsstralung, annihilation and conversion diagrams as shown in Figure 1. The different samples were generated using the following cuts: the dimuon effective mass, $M_{\mu\mu}$, is limited to the range 3 to 40 GeV. The angle between the outgoing muon and the beam axis must be $> 36^o$. The predicted cross sections for different center-of-mass energies are listed in Table 2.

For the background studies, the following event generators are used: KORALZ 4.03 [8] for the ($e^+e^- \to \tau^+\tau^-$) channel, PYTHIA 5.722 [9] for the ($e^+e^- \to ZZ \to$ leptons) channel and LEPWW [10] for the ($e^+e^- \to W^+W^- \to$ leptons) channel.

$e^+e^- \to e^+e^-\tau^+\tau^-$

The $e^+e^- \to e^+e^-\tau^+\tau^-$ events are produced with the JAMVG Monte Carlo [12], which takes into account only the multiperipheral diagram as shown in Fig. 1a. This diagram is sufficient for efficiency calculations since the contribution from other diagrams turns out to be very small. The calculation of the cross section is based on the DIAG36 generator. The background processes are generated with the Monte Carlo programs EGPC [13] for exclusive two-photon processes, PHOJET [14] for $e^+e^- \to e^+e^-q\bar{q}$ and KORALZ for $e^+e^- \to \tau^+\tau^-(\gamma)$.

All generated events are processed through the full L3 detector simulation based on GEANT and GEISHA [15] and are reconstructed following the same procedure used for the data. Time dependent detector inefficiencies, as monitored during the data taking, are also simulated.

4 Event Selection and Data Samples

$e^+e^- \to e^+e^-\mu^+\mu^-$

The muon pairs are selected, using the information from the TEC, the ECAL and the muon chambers. The selection requires:

- Exactly two tracks with at least 12 hits and opposite charges. Each track must have a distance of closest approach smaller than 5 mm to the nominal interaction vertex. The momentum of the tracks must be between 2.5 GeV and 40 GeV.
- Two muons in the muon chambers with at least 2 out of the 3 $r\phi$ layers and 1 out of the 2 z layers.
- Backgrounds from cosmic rays, hadrons decaying in flight and punch-through hadrons are supressed by asking the muon track to point towards the primary vertex and imposing a strict cut on the time of flight.
- The two-photon mass $W_{\gamma\gamma}$ must be between 3 GeV and 40 GeV.

The number of events satisfying these conditions at different center-of-mass energies are shown in Table 1. The total background contribution is found to be $< 1\%$. The Monte-Carlo distributions of the two-photon effective mass and of the momentum of the higher energetic muon in Figure 2a and b agree well with the data.

$e^+e^- \rightarrow e^+e^-\tau^+\tau^-$

The selection of τ pairs, where $\tau^+ \rightarrow \pi^+\pi^0\bar{\nu_\tau}$ and $\tau^- \rightarrow e^-\nu_\tau\bar{\nu}_e$ [1)], is based on the TEC and on the ECAL. The final state particles are observed in the ECAL barrel and endcap regions. The events are mainly accepted by the charged particle trigger [16], which requires at least two charged particles with a transverse momentum p_t >150 MeV, back to back, within an acoplanarity angle of $\pm 41^\circ$ the calorimetric energy trigger [17] and the inner TEC trigger [18]. This last trigger improves the acceptance from $30^\circ < \theta < 150^\circ$ to $15^\circ < \theta < 165^\circ$ and has no requirement on the acoplanarity angle of the tracks.

The events are selected by using the following criteria:

- The total energy in the calorimeters must be less than 40 GeV to exclude annihilation events.
- Exactly two charged tracks are required in the tracking chamber with at least 12 hits per track and opposite charges. For each track, the transverse momentum must be > 0.3 GeV, its distance of closest approach to the interaction point in the transverse plane must be less than 10 mm and there has to be a corresponding signal in ECAL.
- Two neutral particles have to be identified as photons. A photon is defined as an isolated shower in ECAL with an energy larger than 100 MeV distributed over at least two crystals. There must be no track within 150 mrad around the shower direction and the ratio between the energies deposited in HCAL and ECAL must be < 0.2.

The electron identification for the reaction $\tau^- \rightarrow e^-\nu_\tau\bar{\nu}_e$ is based on the energy deposited in ECAL with a shower shape consistent with that of electromagnetic particles. The electromagnetic cluster is required to match with a charged track within 100 mrad in the x-y plane transverse to the beam direction. The momentum of the electron candidate must be > 600 MeV. To achieve high efficency and high purity, the electron identification is based on a neural network [19]. Ten variables are combined in a feed-forward neural network, with one hidden layer and one output node. The input variables include the energy in ECAL, the momentum, the ionisation energy loss in the TEC, the ratio E_t/p_t of the transverse energy in ECAL over the transverse momentum in the TEC, the number of crystals in the shower, two inputs describing the shower shape in ECAL, the energy in HCAL, the energy within a cone of 7 degrees in HCAL and the number of crystals hit in ECAL expected for a minimum ionising particle. As an example, the distribution of the ratio E_t/p_t for data and Monte Carlo events is shown in Figure 3. The agreement is good. A clear signal is observed at E_t/p_t=1 as expected for electrons. The electron identification with the neural network provides an efficiency of $87.7 \pm 0.2\%$ with a purity of $94.7 \pm 0.2\%$ as determined from Monte Carlo events.

To identify $\tau^+ \rightarrow \pi^+\pi^0\bar{\nu_\tau}$ decays, we require one π^0 in addition to a charged particle, which is considered to be the π^+ candidate. No additional selection cuts on the π^+ are applied. The two-photon effective mass distribution in Figure 4a) shows a clear peak at the π^0 mass. A gaussian fit to this peak gives M= 134.6 ± 0.6 MeV and $\sigma = 6.8 \pm 0.7$ MeV, corresponding to the expected mass resolution. We require the two-photon effective mass to be within the range, $115 \leq m(\gamma\gamma) \leq 155$ MeV. To reject exclusive final states, as for example $e^+e^- \rightarrow$

[1)] The charge conjugated process is considered as well

$e^+e^-\mathrm{a}_2(1320) \to e^+e^-\pi^+\pi^-\pi^0$, we require the total transverse momentum imbalance $|\sum \vec{p_t}|$ to be greater than 0.2 GeV. In Figure 4b) the $|\sum \vec{p_t}|$ distribution is compared to the Monte Carlo prediction. The excess of data below $|\sum \vec{p_t}| < 0.2$ values is due to these exclusive two-photon processes. As expected for this τ decay channel, the $\pi^+\pi^0$ effective mass is consistent with the ρ meson mass as shown in Figure 5.

With these criteria, 266 events are selected. The energy distribution of the e^- in the $\tau^- \to e^-\nu_\tau\bar{\nu_e}$ channel and the momentum distribution of the π^+ in $\tau^+ \to \pi^+\pi^0\bar{\nu_\tau}$ channel are shown in Figures 6 and 7. Both distributions are in good agreement with the Monte Carlo simulation.

Table 1 shows the number of observed events for the three energy data sets separately. The main background (26% of the total sample) is due to τ-pairs decaying to other final states, where leptons or pions are misidentified, or additional pions are not detected, whereas the background from resonant final states, $e^+e^- \to e^+e^-q\bar{q}$ and $e^+e^- \to \tau^+\tau^-(\gamma)$ is $< 4\%$. The background from beam-gas and beam-wall interactions is found to be negligible.

5 Results

The total cross section for the two-photon production of lepton pairs is given by

$$\sigma = \frac{N_{\mathrm{obs}} - N_{\mathrm{bkg}}}{\mathcal{L}_l \cdot \epsilon_{\mathrm{trig}} \cdot \epsilon_l \cdot \mathrm{BR}} \tag{2}$$

where

- N_{obs} is the number of observed events in the data,
- N_{bkg} is the number of background events estimated from the Monte Carlo,
- $\mathcal{L}_l$ is the integrated luminosity for the data sample under consideration,
- ϵ_{trig} is the trigger efficiency,
- ϵ_l the lepton pair selection efficiency for the physics analysis. ϵ_{trig} and ϵ_l are given in Table 1.
- BR is the total branching ratio in the case of short lived leptons. For the τ pairs, $\mathrm{BR} = 2 \cdot \mathrm{Br}(\tau^+ \to \pi^+\pi^0\bar{\nu_\tau}) \cdot \mathrm{Br}(\tau^- \to e^-\nu_\tau\bar{\nu_e}) = 9.02 \pm 0.06\%$ [22].

$e^+e^- \to e^+e^-\mu^+\mu^-$

The data collected over the energy range $161 \leq \sqrt{s} \leq 208$ GeV corresponds to an integrated luminosity of 596.1 pb^{-1}.

From the number of events observed and the estimated background contribution the cross section of the process $e^+e^- \to e^+e^-\mu^+\mu^-$ for 3 GeV $< W_{\gamma\gamma} <$ 40 GeV is measured according to Equation 2 in the range $|\cos\theta| < 0.8$. They are given with their statistical and systematic errors for the different $\sqrt{s}$ values in Table 2 and shown in Figure 8a.

To extract the two-photon cross sections for two real photons, $\sigma(\gamma\gamma \to \mu^+\mu^-)$, as a function of $W_{\gamma\gamma}$ as shown in Figure 8b, the number of observed events are corrected in each $W_{\gamma\gamma}$ bin for the two-photon luminosity function [3] and the angular acceptance A:

$$A = \frac{N_{gen}(|cos(\theta)|)}{N_{gen}(|cos(\theta^{*})|)} \tag{3}$$

where $N_{gen}(|cos(\theta)|)$ is the number of events in the angular range $|\cos\theta| < 0.8$ in the e^+e^- center-of-mass system while $N_{gen}(|cos(\theta^*)|)$, with $|\cos\theta^*| < 0.8$ is the number of events in the rest frame of the two gammas. The values obtained at the different $\sqrt{s}$ are consistent within a given $W_{\gamma\gamma}$ bin as shown in Table 3. The systematic errors are given in Table 4. For lower luminosities the error is dominated by the uncertainty on the trigger efficiency. At higher luminosities the main error is coming from limited Monte-Carlo statistics. The error on the event selection has been estimated using data with high integrated luminosity only and is below 1%.

$e^+e^- \to e^+e^-\tau^+\tau^-$

The τ-pair production cross section are computed according to Eq. 2. The detector acceptance and the selection efficiency are determined by JAMVG. Trigger inefficiencies are evaluated directly from the data [21]. A two dimensional trigger inefficiency correction based on the highest momentum track and the azimuthal opening angle between the two tracks is applied. The efficiencies are listed in Table 1. The decrease in the trigger efficiency as a function of $\sqrt{s}$ is due to stricter conditions applied in the years 1999 and 2000 to handle high luminosity at LEP. The total cross section of τ-pair production is given in Table 2 and plotted in Figure 9 together with our previous measurement at 91 GeV [4].

A detailed list of systematic errors is given in Table 4. The main source of systematic error comes from $|\sum \vec{\mathrm{p}_\mathrm{t}}|$ cut. The total systematic error due to selection criteria is estimated to be between 7% to 9% for the three different years of data taking. Other sources of systematic errors are the trigger efficiency uncertainty and the Monte-Carlo statistics, their combined contribution is below 3%. The measured cross-section values of τ-pair production are consistent with $\mathcal{O}(\alpha^4)$ QED calculation by DIAG36 as shown in Figure 9.

The measurement of the anomalous couplings of the τ has been obtained by combining all three measurements into one at a mean energy of 196 GeV, giving $\sigma = 457 \pm 58$ pb. In Figures 10a and b the comparison of the measured cross section with the theoretical calculations [1] for F_2 and d_τ are shown. The calculation of F_2 assumes $d_\tau = 0$ and viceversa. The experimental points are compatible with the Standard Model prediction. From the 1σ bands, the upper limits for F_2 and d_τ can be extracted and are:

$$-0.062 \leq F_2 \leq 0.044 \text{ at } 68\% \text{ CL}$$

$$d_\tau \leq 0.67 \cdot 10^{-15} \text{ at } 68\% \text{ CL}$$

6 Acknowledgements

We would like to thank F. Cornet and J. I. Illana for the helpful discussions.

References

[1] F. Cornet and J. I. Illana, Phys. Rev. D **53** (1996) 1181.

[2] R. Escribano and E. Masso, Phys. Lett. B **395** (1997) 369 R. Engel, Z. Phys. **C 66** (1995) 203;
R. Engel and J. Ranft, PR **D 54** (1996) 4246.

[3] G.A. Schuler,hep-ph/9610406.

[4] L3 Coll., M. Acciari et al., Phys. Lett. **B 403** (1997) 168.

[5] OPAL Coll., R. Akers et al., Zeit. fur Physik **C 60** (1993) 593.

[6] L3 Coll., B. Adeva et al., Nucl. Instr. and Meth. **A 289** (1990) 35;
M. Acciarri et al., Nucl. Instr. and Meth. **A 351** (1994) 300;
M. Chemarin et al., Nucl. Instr. and Meth.**A 349** (1994) 345;
A. Adam et al., Nucl. Instr. and Meth. **A 383** (1996) 342.

[7] F.A. Berends, P.H. Daverveldt and R. Kleiss. Comp. Phys. Com. **40** (1986) 285.

[8] KORALZ version 4.02 is used;
S. Jadach, B.F.L. Ward and Z. Was, Comp. Phys. Comm. **79** (1994) 503.

[9] PYTHIA 5.772, T. Sjöstrand, Comp. Phys. Com. **82** 74 (1994).

[10] WW generator report of the LEP2 workshop, hep-ph/9709270. See also *Physics at LEP2*, editors: G. Altarelli, T. Sjöstrand and F. Zwirner, CERN 96-01.

[11] R. Brun et al., GEANT 3.15 preprint CERN DD/EE/84-1 (1984), revised 1987.

[12] J.A.M. Vermaseren, Nucl. Phys. **B 229** (1983) 347.

[13] F. Linde, "Workshop on detector and event simulation in high energy physics Monte Carlo", eds. K. Bos and B. van Eijl, Amsterdam, 1991.

[14] PHOJET version 1.05c is used.

[15] H. Fesefeldt, RWTH Aachen report PITHA 85/2 (1985).

[16] P. Béné et al., NIM **A 306** (1991) 150.

[17] R. Bizzarri *et al.*, NIM **A 283** (1989) 799.

[18] D. Haas et al., NIM **A 420** (1999) 101 - 116.

[19] Stuttgart Neural Network Simulator, http://www-ra.informatik.uni-tuebingen.de/SNNS/

[20] V.M. Budnev *et al.,* Physics Reports **15** 181 (1975).

[21] D. Haas, PhD Thesis, University of Basel, Basel, 2000.

[22] The European Physical Journal C (1998) Volume 3, 1-4.

$\ell^+\ell^-$	$<\sqrt{s}>$ (GeV)	$\int \mathcal{L}dt$ (pb)	ϵ_ℓ (%)	ϵ_{trig} (%)	$\mathrm{N_{obs}}$	$\mathrm{N_{bkg}}$
$\mu^+\mu^-$	161	10.2	18.4 ± 0.5	99.4 ± 0.6	193	4
	172	9.7	18.9 ± 0.5	98.4 ± 0.8	223	7
	183	54.2	18.4 ± 0.3	99.7 ± 0.2	1188	15
	189	170.3	20.1 ± 0.3	99.6 ± 0.1	4025	33
	196	154.0	18.9 ± 0.3	99.7 ± 0.1	3491	36
	206	192.7	19.1 ± 0.2	99.7 ± 0.1	4576	45
$\tau^+\tau^-$	189	172.1	1.18 ± 0.04	71.8 ± 1.3	85.0	24.7
	196	220.9	1.29 ± 0.05	60.1 ± 1.6	97.0	31.0
	206	215.1	1.08 ± 0.04	58.0 ± 0.9	84.0	28.5

Table 1: Center-of-mass energies and corresponding integrated luminosities of the data samples used for this analysis. Also given are the selection efficiency ϵ_ℓ and trigger efficiency ϵ_{trig} together with the number of observed events and the background contribution.

$\ell^+\ell^-$	$<\sqrt{s}>$ [GeV]	σ [pb] (MC)	σ [pb] (DATA)
$\mu^+\mu^-$	161	113.0	$101.4 \pm 7.2 \pm 2.6$
	172	115.4	$119.2 \pm 7.6 \pm 3.1$
	183	116.9	$117.7 \pm 3.4 \pm 1.9$
	189	117.7	$117.1 \pm 1.8 \pm 1.8$
	196	118.9	$118.9 \pm 2.0 \pm 2.2$
	206	120.5	$122.6 \pm 1.8 \pm 1.7$
$\tau^+\tau^-$	189	442.6	$459 \pm 68 \pm 33$
	196	452.3	$454 \pm 67 \pm 42$
	206	466.0	$459 \pm 76 \pm 35$

Table 2: The cross-sections ($\sigma(DATA)$) of the processes $e^+e^- \to e^+e^-\mu^+\mu^-$ and $e^+e^- \to e^+e^-\tau^+\tau^-$ with its statistical and systematic errors at different center-of-mass energies compared to the DIAG36 [7] expectations ($\sigma(MC)$). The cross section for $e^+e^- \to e^+e^-\mu^+\mu^-$ is given within the kinematical region defined in the text.

$W_{\gamma\gamma}$ interval	$\sigma_{\gamma\gamma}$ [nb] (183 GeV)	$\sigma_{\gamma\gamma}$ [nb] (189 GeV)	$\sigma_{\gamma\gamma}$ [nb] (196 GeV)
3 GeV – 4 GeV	14.10 ± 3.93	15.63 ± 2.19	14.51 ± 2.44
4 GeV – 5 GeV	11.17 ± 1.32	11.53 ± 0.72	11.97 ± 0.80
5 GeV – 6 GeV	9.18 ± 0.60	8.55 ± 0.32	9.95 ± 0.39
6 GeV – 7 GeV	7.39 ± 0.49	7.68 ± 0.28	8.44 ± 0.33
7 GeV – 8 GeV	6.05 ± 0.51	6.99 ± 0.30	7.59 ± 0.36
8 GeV – 10 GeV	5.40 ± 0.39	5.55 ± 0.22	6.13 ± 0.26
10 GeV – 15 GeV	4.53 ± 0.33	3.93 ± 0.16	4.20 ± 0.18
15 GeV – 20 GeV	2.79 ± 0.34	2.64 ± 0.18	3.16 ± 0.23
20 GeV – 40 GeV	1.27 ± 0.17	1.31 ± 0.10	1.24 ± 0.10

Table 3: The cross section for two real photons $\sigma(\gamma\gamma \to \mu^+\mu^-)$ with its combined statistical and systematic error as a function of $W_{\gamma\gamma}$ for three different energies.

$\ell^+\ell^-$	Source of Systematics	161 GeV	172 GeV	183 GeV	189 GeV	196 GeV	206 GeV
$\mu^+\mu^-$	Event Selection	0.75%	0.75%	0.75%	0.75%	0.75%	0.75%
	Trigger	3.0%	2.8%	0.33%	0.20%	0.21%	0.21%
	Monte Carlo statistics	2.4%	2.4%	1.4%	1.3%	1.7%	1.2%
	Total	3.9%	3.8%	1.6%	1.5%	1.9%	1.4%
$\tau^+\tau^-$	Event selection				7.1 %	8.8 %	7.2 %
	Trigger Level 1				1.7 %	2.7 %	1.4 %
	Higher Level Trigger				0.4 %	0.4 %	0.4 %
	Monte Carlo statistics				1.5 %	1.5 %	1.5 %
	Total				7.5 %	9.3 %	7.5 %

Table 4: Uncertainties on $\sigma(e^+e^- \to e^+e^-\mu^+\mu^-)$ and $\sigma(e^+e^- \to e^+e^-\tau^+\tau^-)$ for the different sets of data.

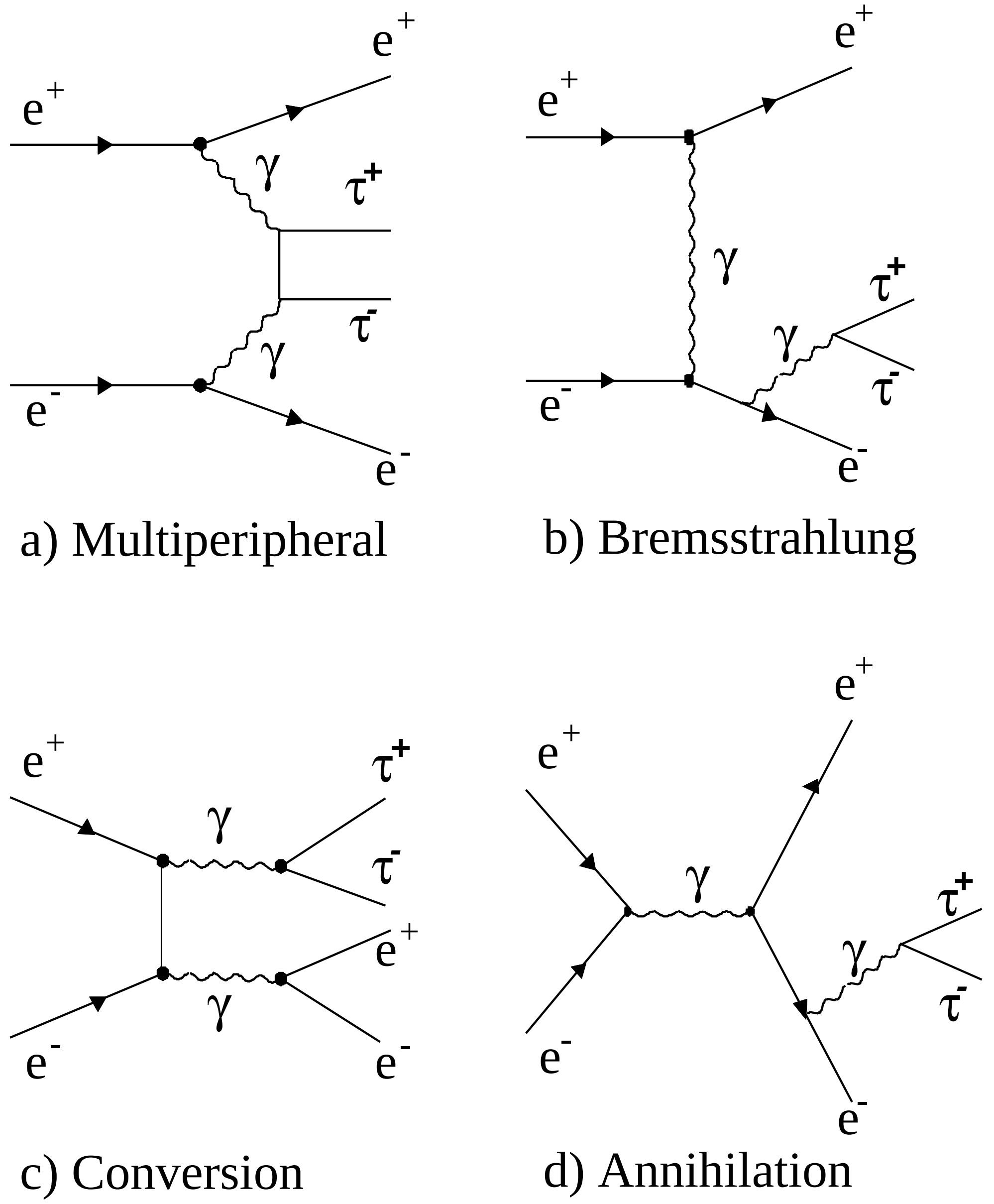

Figure 1: Principal Feynman graphs at $\mathcal{O}(\alpha^4)$ of the process $e^+e^- \rightarrow e^+e^-\tau^+\tau^-$: a) Multiperipheral, b) Bremsstrahlung, c) Conversion, d) Annihilation

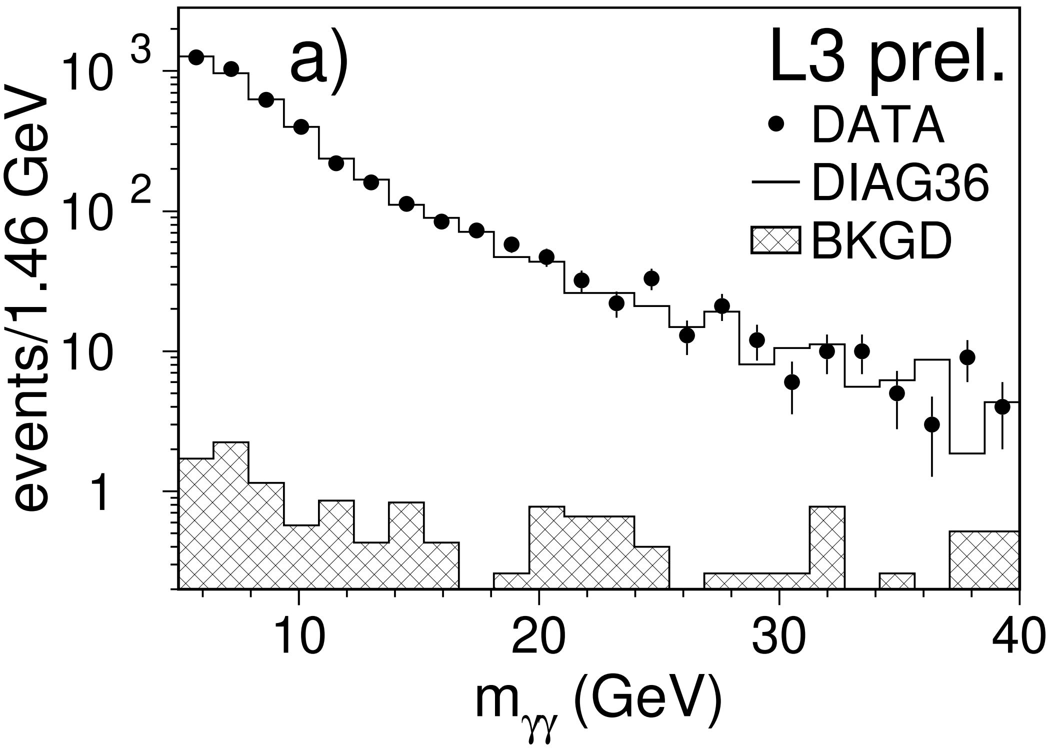

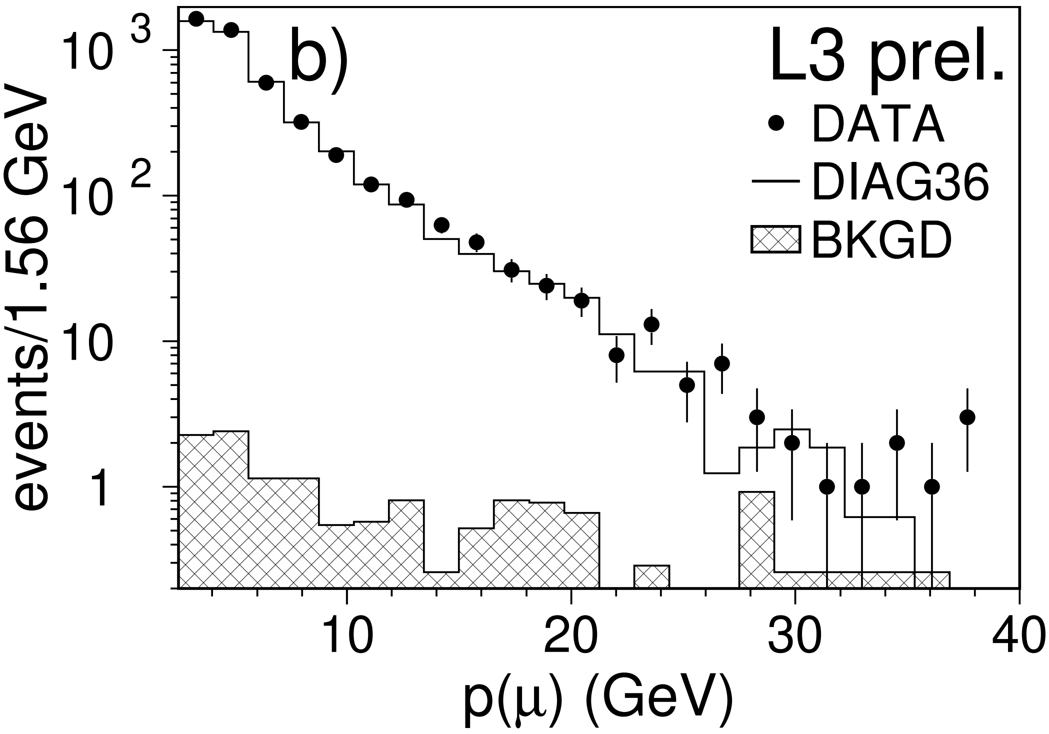

Figure 2: (a) The mass distribution $m_{\gamma\gamma}$. (b) The momentum of the most energetic muon $p(\mu)$. The data are compared to the predictions of the DIAG36 Monte Carlo for $\mathrm{e}^+e^- \rightarrow e^+e^-\mu^+\mu^-$. The background (see text) is shown as a hatched histogram. The predictions are normalized to the integrated luminosity of the data.

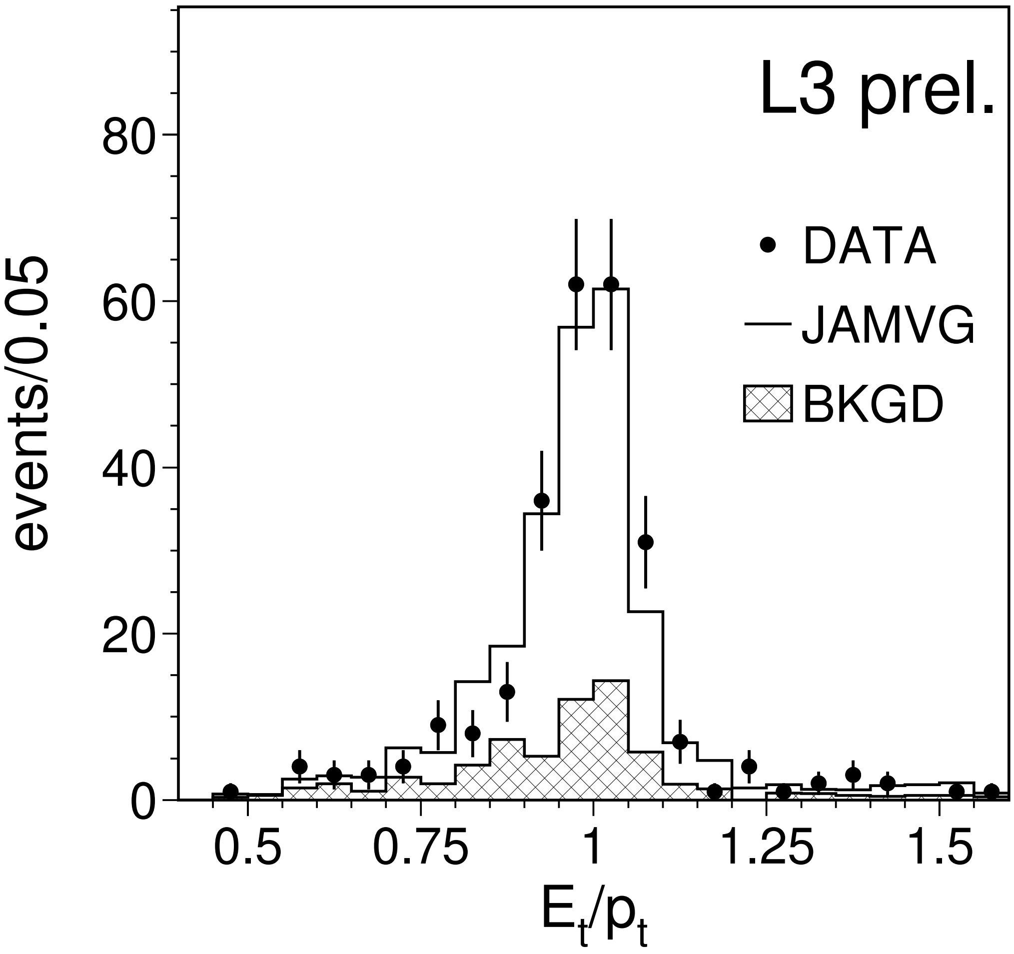

Figure 3: The ratio of the transverse energy measured in the electromagnetic calorimeter and the transverse momentum measured in the central chamber for the electron, E_t/p_t after all cuts. The data are compared to the predictions of the JAMVG Monte Carlo for $e^+e^- \to e^+e^-\tau^+\tau^-$, $\tau^+ \to \pi^+\pi^0\bar{\nu_\tau}$, $\tau^- \to e^-\nu_\tau\bar{\nu}_e$ (solid line). The dominant background from other τ-decays together with exclusive resonant states, $e^+e^- \to e^+e^-q\bar{q}$ and $e^+e^- \to \tau^+\tau^-(\gamma)$ is shown as a hatched histogram. The predictions are normalized to the integrated luminosity of the data.

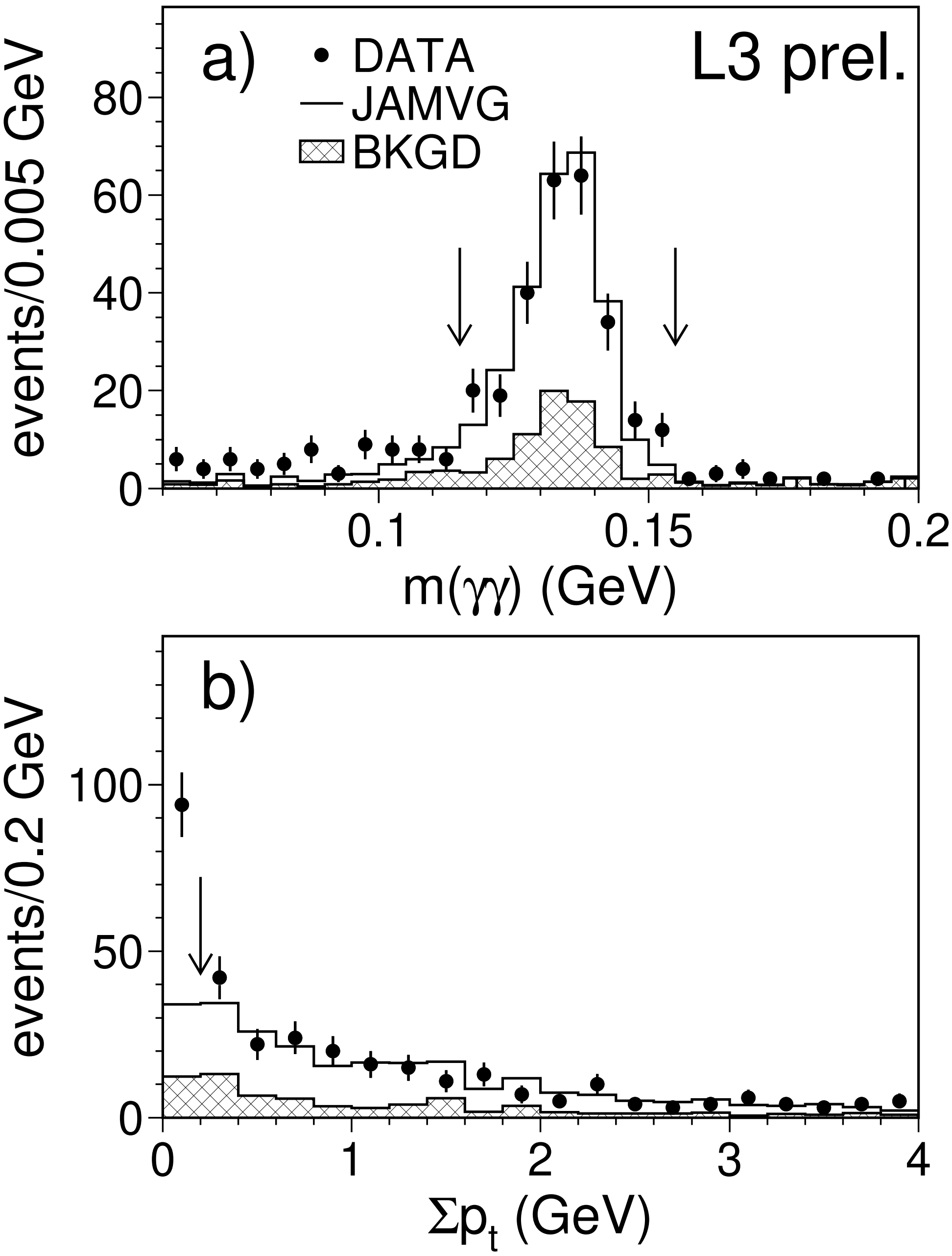

Figure 4: (a) Effective mass distribution $m(\gamma\gamma)$ of final state photons; the arrows indicate the cuts at 115 MeV and 155 MeV defining the π^0 signal region. (b) The sum of the transverse momenta of the final charged particles, $|\sum \vec{p_t}|$; the arrow indicates the cut at 0.2 GeV which suppresses exclusive resonant two-photon channels. The data are compared to the JAMVG Monte Carlo $e^+e^- \to e^+e^-\tau^+\tau^-$ (solid line) and the background (hatched) normalized to the integrated luminosity. The combined data sample from 189 - 208 GeV is shown. All selection cuts are fulfilled, except the one on the plotted variable.

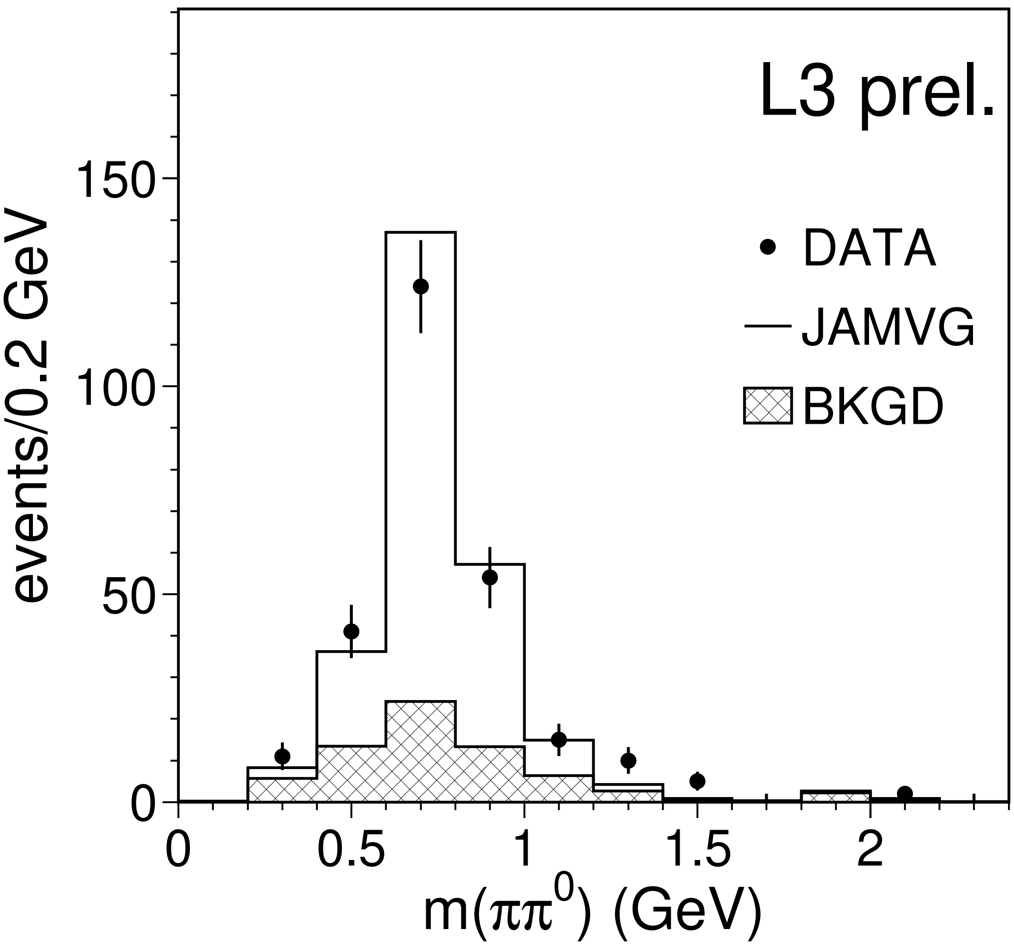

Figure 5: The distribution of the mass m($\pi^+\pi^0$) signing the decay $\tau^+ \rightarrow \rho^+\bar{\nu_\tau} \rightarrow \pi^+\pi^0\bar{\nu_\tau}$. The data are compared to the JAMVG Monte Carlo $e^+e^- \rightarrow e^+e^-\tau^+\tau^-$ (solid line) and the background (hatched) normalized to the integrated luminosity. The combined data sample from 189 - 208 GeV is shown.

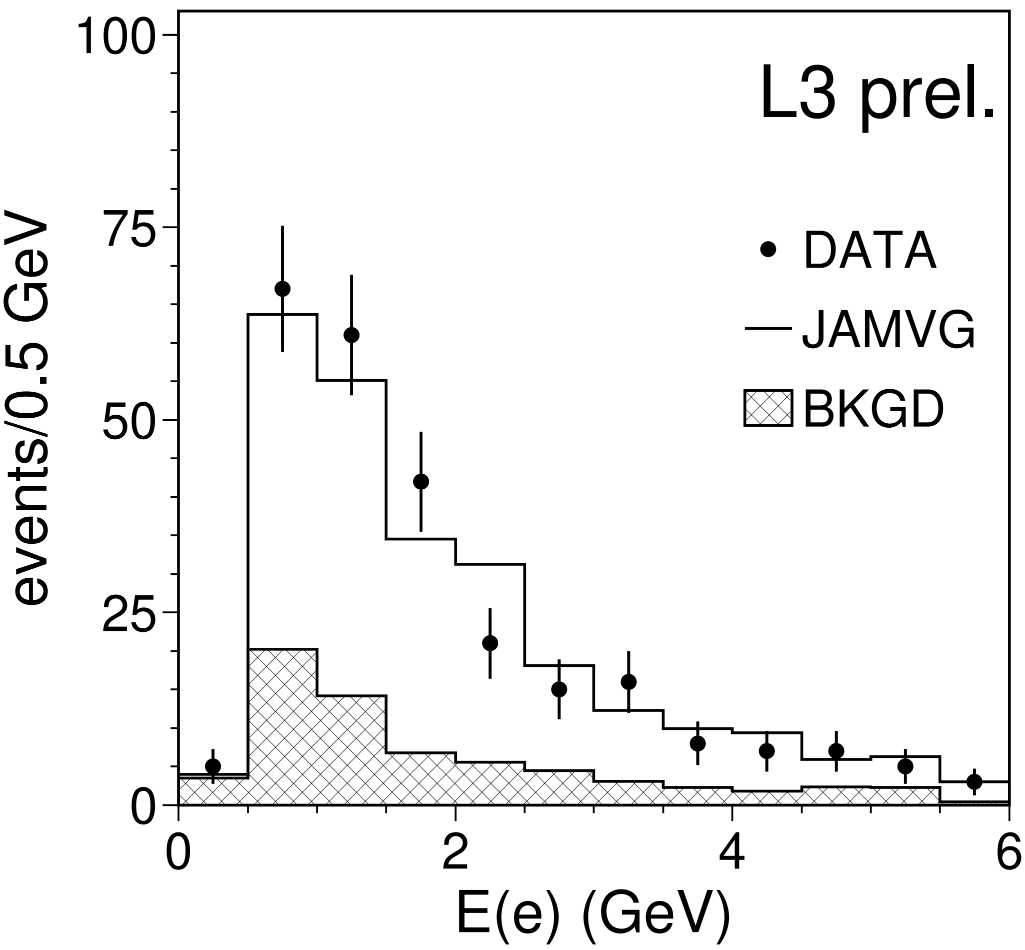

Figure 6: The distribution of the energy of the electron deposited in the electromagnetic calorimeter. The data are compared to the JAMVG Monte Carlo $e^+e^- \rightarrow e^+e^-\tau^+\tau^-$ (solid line) and the background (hatched) normalized to the integrated luminosity. The combined data sample from 189 - 208 GeV is shown.

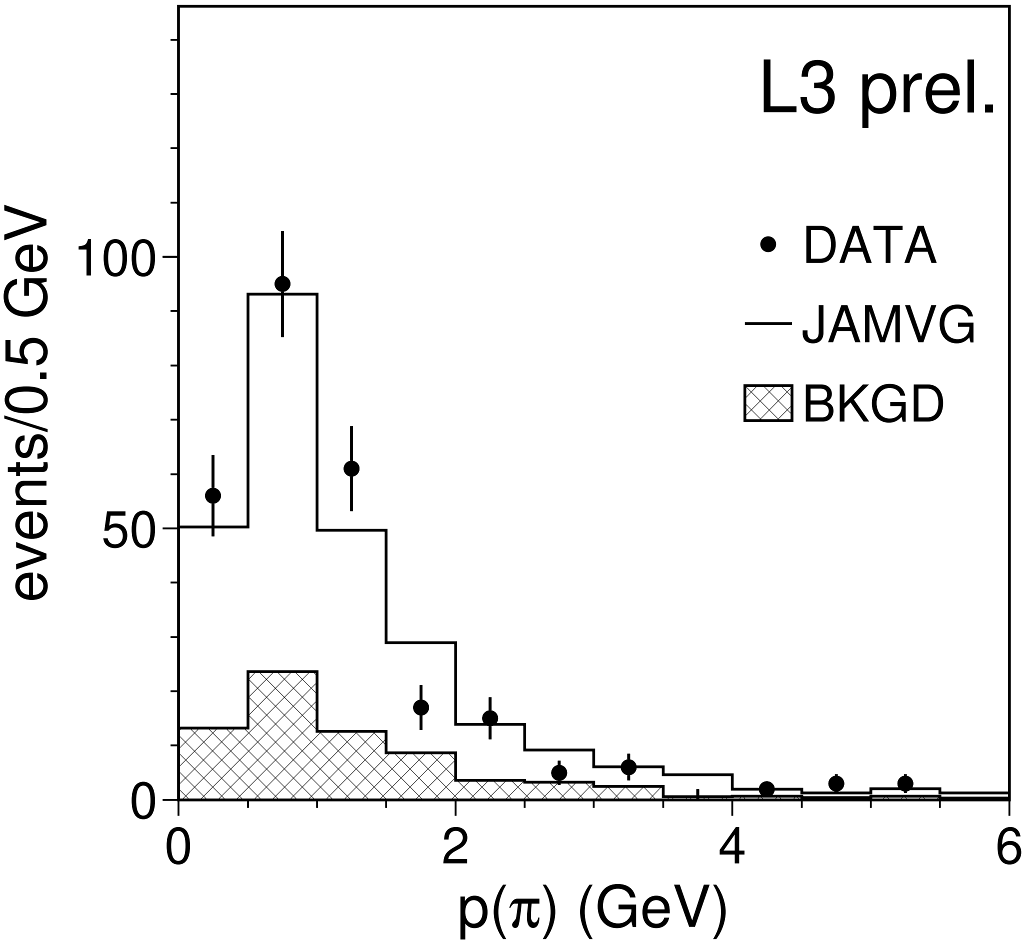

Figure 7: Charged pion momentum distribution. The data are compared to the JAMVG Monte Carlo $e^+e^- \rightarrow e^+e^-\tau^+\tau^-$ (solid line) and the background (hatched) normalized to the integrated luminosity. The combined data sample from 189 - 208 GeV is shown.

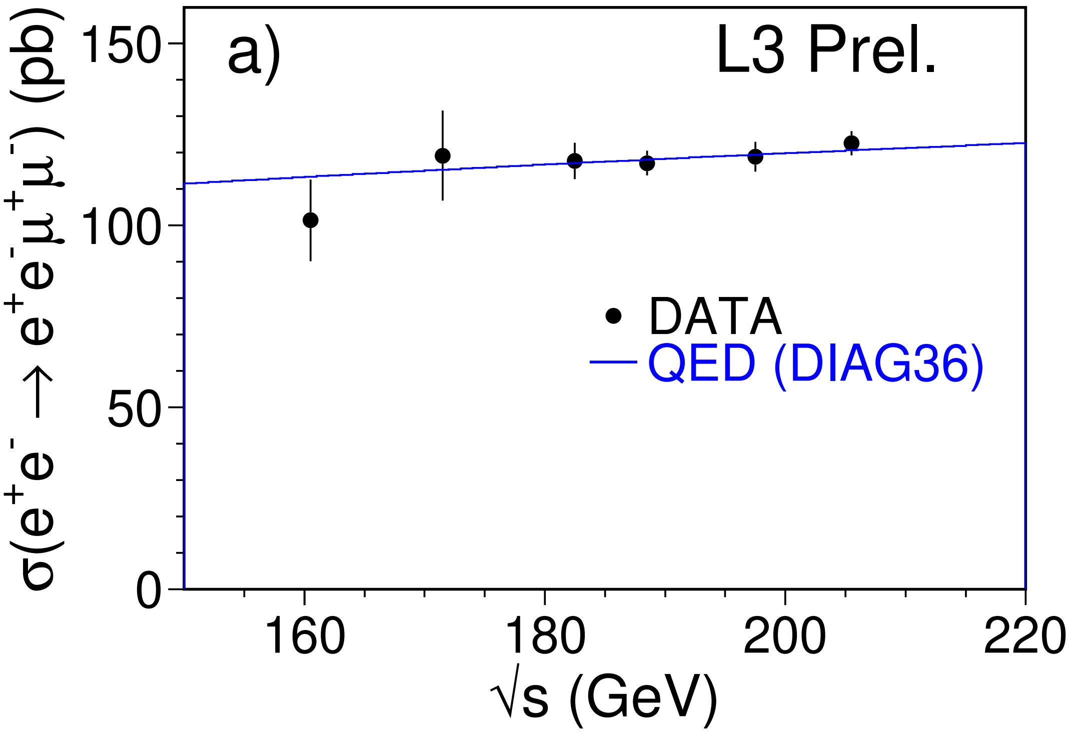

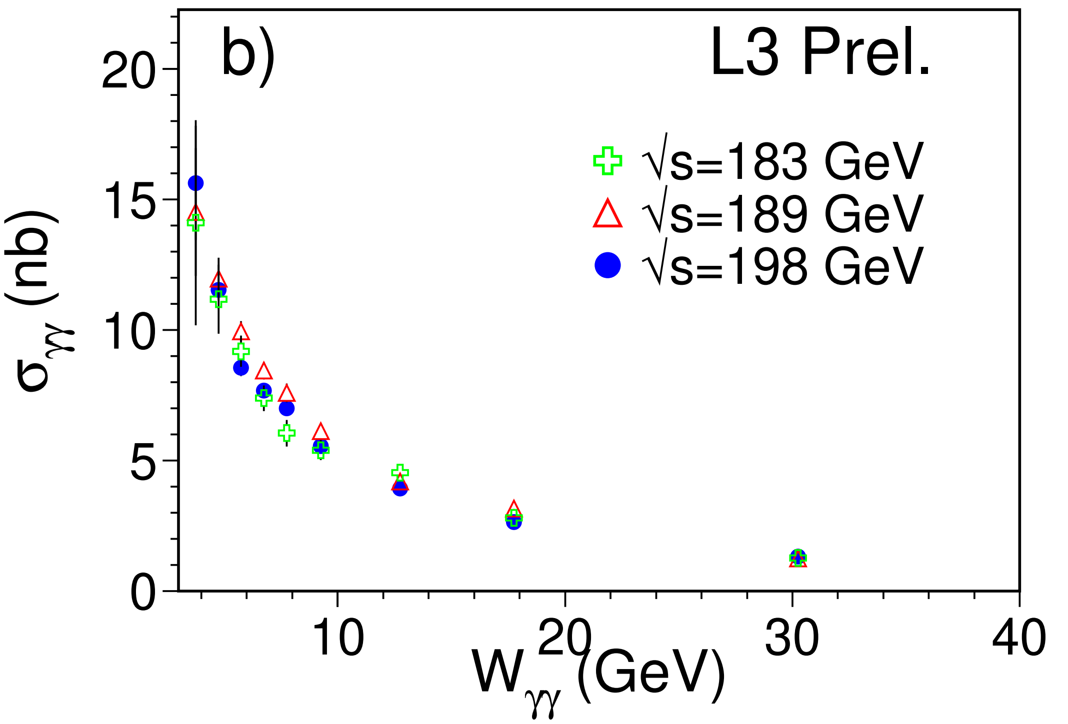

Figure 8: (a) The cross section $\sigma(e^+e^- \to e^+e^-\mu^+\mu^-)$ as a function of $\sqrt{s}$ in the kinematical range as described in the text. The data are compared to DIAG36 predictions. (b) The cross section $\sigma_{\gamma\gamma} = \sigma(\gamma\gamma \to \mu^+\mu^-)$ for two real photons as a function of the $\gamma\gamma$ mass for the three energies indicated.

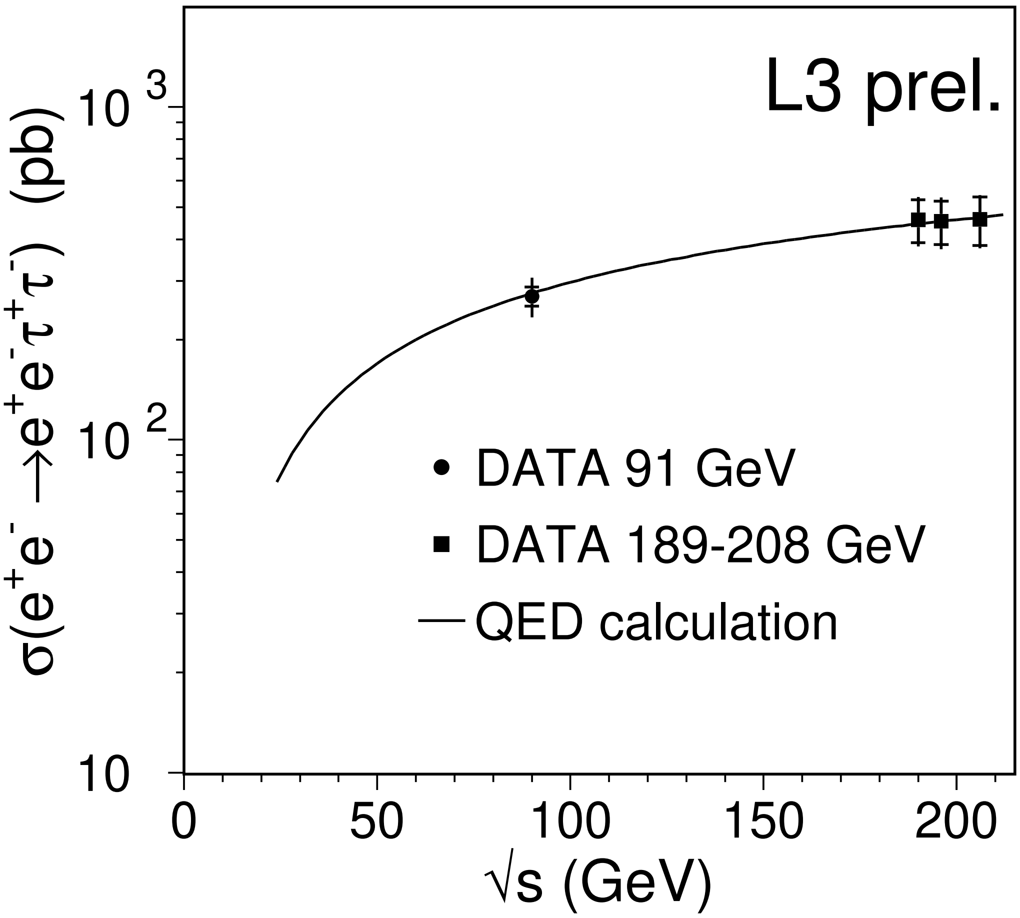

Figure 9: The cross section $\sigma(e^+e^- \to e^+e^-\tau^+\tau^-)$ as a function of $\sqrt{s}$. The data are compared to QED calculations of DIAG36.

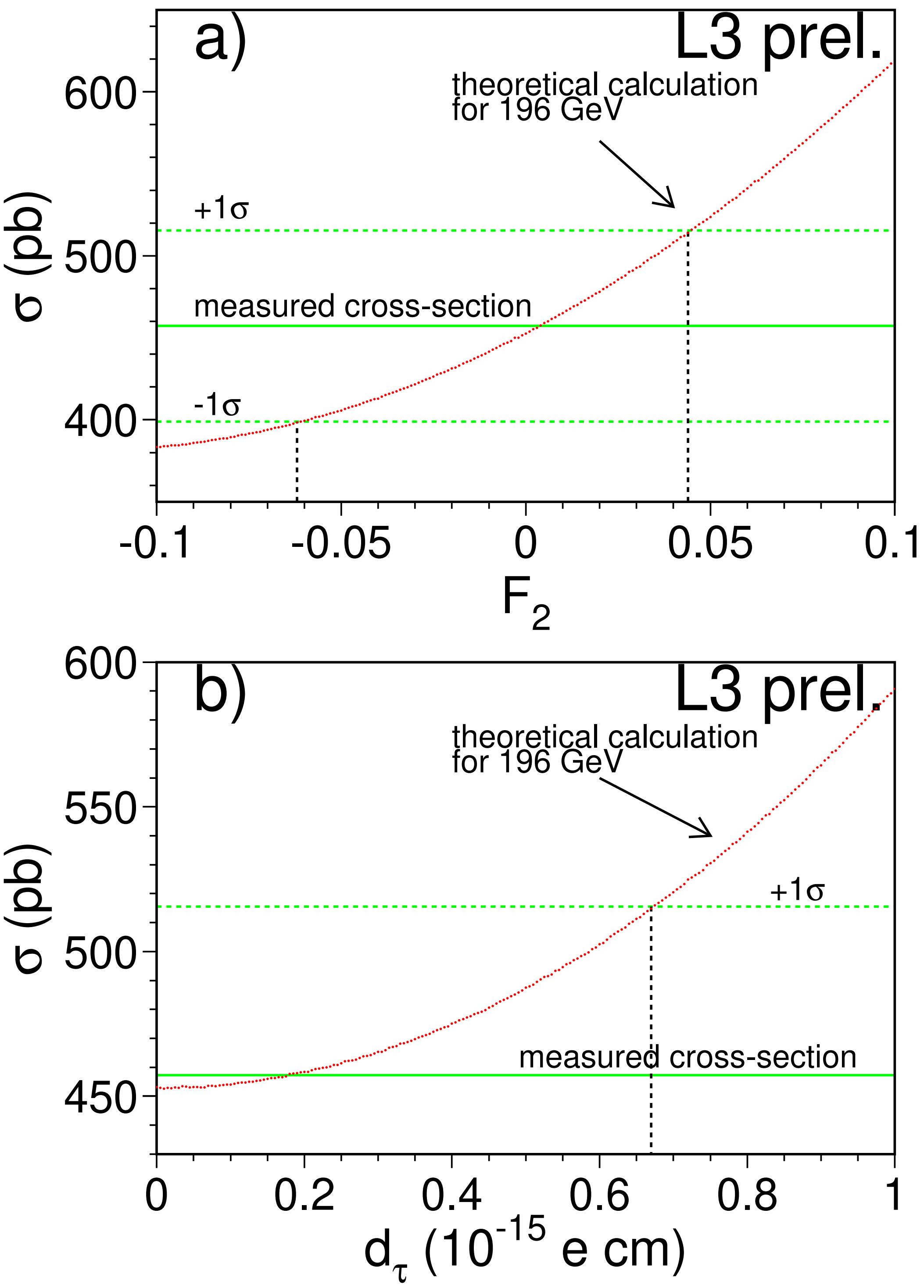

Figure 10: Comparison of the measured cross-section with theoretical calculations: a) F_2 in the presence of an anomalous magnetic moment. b) d_τ in the presence of an anomalous electric moment.